

All-Inorganic Hetero-Structured Cesium Tin Halide Perovskite Light-Emitting Diodes With Current Density Over 900 A cm^{-2} and Its Amplified Spontaneous Emission Behaviors

Fang Yuan, Jun Xi, Hua Dong, Kai Xi, Wenwen Zhang, Chenxin Ran, Bo Jiao, Xun Hou, Alex K.-Y. Jen,* and Zhaoxin Wu*

Pursuing novel new materials for fabricating efficient electrically pumped lasers is the emphasis of researchers for decades. Although organic semiconductors with high gain have been reported previously, a significant challenge remains in using them for electrically pumped lasers due to their low carrier mobility. Recently, hybrid halide perovskites have been reported to possess high carrier mobility and optical gain which allows them to be used for various optoelectronic applications. To explore the feasibility of using them as possible candidates for electrically pumped lasers, tin (Sn)-based perovskite light-emitting diodes (PeLEDs) with all-inorganic heterostructure are fabricated by the vapor-deposition process. The all-inorganic heterostructured PeLEDs exhibited a maximum EQE of $\approx 0.34\%$, and withstood current density up to 915 A cm^{-2} with small emission zone of 0.01 mm^2 . In addition, by vacuum vapor deposition, extremely smooth and uniform cesium tin halide perovskite films with small grain size ($\approx 60 \text{ nm}$) are obtained, in which low threshold ($\approx 7 \mu\text{J cm}^{-2}$) of their amplified spontaneous emission was presented. These characteristics demonstrate the great potential of using them as gain media for electrically pumped lasers.

components, it is very critical to develop efficient growth and processing of semiconductor emitters for realizing electrically driven lasers.^[6,7] However, the conventional semiconductor materials that have been developed so far usually possess certain flaws such as the low carrier mobility in organic semiconductors and the rigid preparation techniques for inorganic semiconductors.^[7,8] Furthermore, most of the inorganic semiconducting emitters contain toxic elements such as arsenide and cadmium, which causes certain health and environmental concerns.^[1,2] Therefore, it is imperative to develop new semiconductor materials with nontoxic elements and high photoluminescence (PL) quantum efficiency and optical gain in order to realize electrically pumped lasers.

Recently, hybrid metal halide perovskites have been extensively studied for photovoltaic and optoelectronic applications because of their attractive synthetic tunability, low production cost, high absorption coefficient, balanced charge transport, and long charge carrier diffusion lengths.^[9–15] Current state-of-the-art perovskite solar cells achieved a certified power

The possibility of developing efficient on-chip coherent light sources from electrically pumped semiconductor laser diodes (LDs) has been the center of attention for researchers in the integrated optoelectronic field.^[1–5] As one of the key

tions because of their attractive synthetic tunability, low production cost, high absorption coefficient, balanced charge transport, and long charge carrier diffusion lengths.^[9–15] Current state-of-the-art perovskite solar cells achieved a certified power

Dr. F. Yuan, Dr. J. Xi, Dr. H. Dong, Dr. C. Ran, Dr. B. Jiao, Prof. X. Hou, Prof. Z. Wu
Key Laboratory for Physical Electronics and Devices of the Ministry of Education & Shaanxi Key Lab of Information Photonic Technique
School of Electronic and Information Engineering
Xi'an Jiaotong University
No.28, Xianning West Road, Xi'an 710049, China
E-mail: zhaoxinwu@mail.xjtu.edu.cn


Prof. A. K.-Y. Jen
Department of Materials Science and Engineering
University of Washington
Seattle, WA 98195, USA
E-mail: ajen@uw.edu

K. Xi
Department of Materials Science and Metallurgy
University of Cambridge
Cambridge CB3 0FS, UK

W. Zhang
School of Electronic Engineering,
Xi'an University of Post & Telecommunication
Xi'an 710121, China

Prof. A. K.-Y. Jen
Department of Materials Science & Engineering
City University of Hong Kong
Kowloon 999077, Hong Kong

Z. Wu
Collaborative Innovation Center of Extreme Optics
Shanxi University
Taiyuan 030006, China

 The ORCID identification number(s) for the author(s) of this article can be found under <https://doi.org/10.1002/pssr.201800090>.

DOI: 10.1002/pssr.201800090

conversion efficiency of 22.1% and the efficient perovskite light-emitting diodes (PeLEDs) exhibited a record external quantum efficiency (EQE) of 11.7%.^[16,17] The general formula of these hybrid halide perovskites is ABX_3 (where A is for a monovalent cation, B is for a divalent metal ion, and X is for a halide anion). So far, the majority of these perovskites studied are focused on the lead-based perovskites, $APbX_3$, where $CH_3NH_3^+$ or $HC(NH_2)_2^+$ is the commonly used cation. Although the performance of photovoltaic devices is quite promising, the toxicity associated with Pb is a serious concern that needs to be addressed. As a more environmentally friendly alternative to Pb^{2+} , Sn^{2+} is a less toxic divalent cation that has drawn quite some attention lately.^[18–21] Although the performance of Sn-based perovskites investigated so far is inferior to their Pb-based counterparts, and they also encounter severe stability problems due to the susceptibility of tin oxidation,^[22–27] these $CsSnX_3$ perovskites possess considerably attractive optoelectronic properties, such as high PL quantum yield, optical gain, and carrier mobility.^[20,21,28] Especially, the high carrier mobility as high as $585\text{ cm}^2\text{ V}^{-1}\text{ s}^{-1}$ enable them to be considered for use in electrically pumped lasing diodes.^[28] In order to explore the feasibility of electrically pumped LDs based on perovskite materials, the biggest issue we confront is the current density required for lasing. This issue could be considered as two parts: one is the minimum current density required reaching lasing threshold; the other is the maximum current density passed through the PeLEDs, owing to the architecture of LDs being usually developed from PeLEDs. Only if the current density through the PeLEDs is above the required minimum current density for lasing, the electrically pumped lasing can be feasible. If the additional losses are not taken into account, the threshold current density for electrically pumped LDs is generally estimated from the lasing threshold of the gain media. Apparently, electrically pumped LDs would be implemented more easily in a low lasing threshold system, which means that reducing the lasing threshold of perovskite materials is a motivating goal. In addition, for PeLEDs with the sandwiched structure, however, the smooth, full coverage and dense $CsSnX_3$ films with high quality are highly desirable, which guarantees the perfect planar waveguide and a low amplified spontaneous emission (ASE) threshold. For the high current tolerance of devices, an all-inorganic architecture of PeLEDs including inorganic hole and electron transport layers should be developed, which could endure as high current density as possible.

In our study, an all-inorganic hetero-structured PeLED based on $CsSnBr_3$ is demonstrated by all vacuum vapor-deposition, which exhibited a maximum EQE of $\approx 0.34\%$, and could sustain high current density up to 915 A cm^{-2} with the small emission zone as 0.01 mm^2 . In our experiment, thin SnX_2 and CsX films are sequentially deposited by vapor deposition then thermal annealed to form uniform cesium tin halide perovskite films through inter-diffusion. Extremely smooth, uniform and full coverage $CsSnX_3$ films with very small grain size of about 60 nm were achieved, which show the low threshold ($\approx 7\text{ }\mu\text{J cm}^{-2}$) ASE and tunable lasing emissions in broader wavelengths (697–923 nm) through different halogen substitutions. These combined desirable characteristics of electrically pumped spontaneous emission and optically pumped ASE are important requisites needed for demonstrating electrically pumped lasing diodes.

Because of rapid crystallization of $CsSnX_3$, the morphology and quality of $CsSnX_3$ films by solution process are usually poor, which do not favor to the planar waveguide structure, and then lasing behaviors. Herein, the vapor deposition process is used for the fabrication of $CsSnX_3$ films, illustrated in **Figure 1a**. As an example, the film of $CsSnBr_3$ was prepared by sequential deposition of $SnBr_2$ (50 nm) and $CsBr$ (45 nm) in a vacuum chamber at a rate of $\approx 0.4\text{--}0.5\text{ }\text{Å s}^{-1}$ under a pressure of $1 \times 10^{-3}\text{ Pa}$. After deposition, the substrates were transferred into a nitrogen-filled glovebox and then annealed at $100\text{ }^\circ\text{C}$ for 60 min. The stacked precursor layers start to interact with each other after deposition, and the final perovskite layer is formed when the inter-diffusion of elements via thermal annealing is finished.^[29] The Scanning Electron Microscopy (SEM) picture of the $CsSnBr_3$ film is shown in **Figure 1b**. It has a complete coverage of the whole substrate surface without any pinholes, with the grain sizes in the range of $\approx 50\text{--}85\text{ nm}$. **Figure 1c** shows the surface topography of $CsSnBr_3$ film by measuring with Atomic Force Microscopy (AFM). The film morphology is very smooth compared to those generated from solution processed films. It has a root mean square (RMS) surface roughness of $\approx 3.8\text{ nm}$ in the $5 \times 5\text{ }\mu\text{m}^2$ area. The other $CsSnX_3$ films generated through different halogen precursors also show relatively smooth film topography. However, the films derived from chloride ions are rougher mainly due to the instability of chloride-based perovskites (**Figure S1**, in Supporting Information).

The $CsSnX_3$ perovskite films display a orthorhombic or cubic phase (**Figure 1d**). The corresponding X-ray diffraction (XRD) of the as-prepared $CsSnX_3$ ($CsSnCl_3$, $CsSnClBr_2$, $CsSnBr_3$, $CsSnBrI_2$, and $CsSnBr_{0.5}I_{2.5}$) films on glass substrates are shown in **Figure 1e**. It is quite clear that both bromide and iodide ions form orthorhombic (Pnma) perovskite crystal structures of lower symmetry while the chloride ions produce a cubic space group (Pm3m).^[30] Due to complete reaction from the inter-diffusion process, these vapor deposited all-inorganic $CsSnX_3$ films possess excellent crystalline properties of perovskite structures, which is very beneficial for future optimization of these $CsSnX_3$ -based devices.

Another huge advantage for these $CsSnX_3$ perovskites is the bandgap tunability through different halide substitution. By using mixtures of either chlorides, bromides or iodides, the bandgap is completely tunable from visible to near-IR region (from ≈ 420 to 915 nm). **Figure 1f** shows the normalized thin-film absorption and PL spectra of $CsSnCl_3$, $CsSnClBr_2$, $CsSnBr_3$, $CsSnBrI_2$, and $CsSnBr_{0.5}I_{2.5}$, demonstrating the tunability of broad wavelengths. When the composition of the $CsSnX_3$ films is varied from Cl to Br and to I, the absorption edge is red-shifted from 2.95 to 1.35 eV, with color of the perovskite films also significantly changed from light grey for $CsSnCl_3$ to reddish brown for $CsSnBr_3$, and black brown for $CsSnBr_{0.5}I_{2.5}$. The atomic ratio for all the prepared compositions was confirmed through careful EDX analysis. In addition, photoluminescence quantum efficiency (PLQE) for the $CsSnBr_3$ film is measured to be as large as $9 \pm 2\%$ which is comparable for the lead-based perovskites and comparatively smaller values (7–1%) for the other $CsSnX_3$ films are obtained mainly derived from increased trap state density induced by halogen substitution. It is important to note that phase-pure $CsSnI_3$ perovskite could not be obtained using the method described in our experiments.

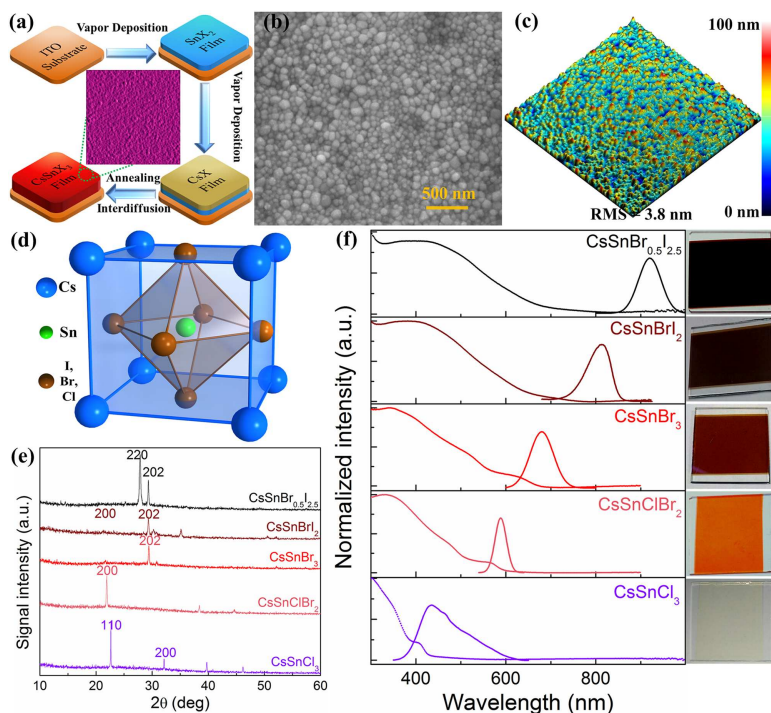


Figure 1. a) Schematic illustration of the fabrication procedure of the CsSnX₃ films prepared by vapor deposition. b) Top view SEM image of the CsSnBr₃ film. c) 3D AFM image of the CsSnBr₃ film. d) The typical CsSnX₃ perovskite atomic crystal structure. e) Bragg-Brentano X-ray diffraction patterns for CsSnX₃ films. f) Normalized absorption spectra and steady-state PL spectra of CsSnX₃ films containing pure and mixed halides.

CsSnI₃ is not stable as a perovskite phase at room temperature, but is stable at high temperature.^[31] The CsSnI₃ obtained from vapor deposition may undergo a phase transition during sample cooling or the course of measurement.

To obtain insight of the inter-diffusion process and to investigate the stability of CsSnX₃ films prepared by vapor deposition, the absorption and PL spectra of freshly prepared and annealed CsSnBr₃ films were examined. As shown in **Figure 2a**, the fresh SnBr₂/CsBr film right after vapor deposition, displays weaker absorption in the visible region than that of the annealed sample. The color of the fresh SnBr₂/CsBr film changes from yellow to reddish brown after being

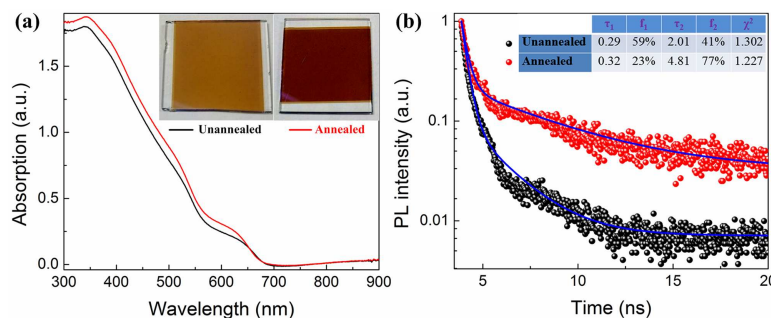


Figure 2. a) The absorption spectra and the images of the un-annealed (black line) and annealed (red line) CsSnBr₃ films. b) Time-resolved PL decay kinetics of the un-annealed (black dots) and annealed (red dots) CsSnBr₃ films.

annealed. Herein, the SnBr₂ and CsBr have partially reacted to form CsSnBr₃ after evaporation because of their strong chemical reactivity. These two layers then completely react to form the perovskite layer through the inter-diffusion process.

The PL intensity of this annealed sample is much stronger than that of the fresh sample, and it only decreased slightly after being exposed to air for 60 min, confirming the relatively good stability of these CsSnX₃ films (Figure S2, in Supporting Information). It has been previously reported that oxidation of Sn²⁺ to Sn⁴⁺ will increase nonradiative carrier recombination and lower PL intensity of Sn-based perovskites.^[22,32] In addition, time-resolved photoluminescence (TRPL) measurements were conducted to further explore the reaction mechanism and PL performance of these CsSnX₃ films. As clearly shown in Figure 2b, PL decay curves were fitted with a biexponential decay model. The bimolecular recombination lifetime of the annealed CsSnBr₃ film is about 4.8 ns, which is much longer than that of the unannealed one. This is mainly owing to the PL quenching by the subjacent SnBr₂ layer in the unannealed sample. Furthermore, to confirm the thermal stability of CsSnBr₃ quantitatively, the thermogravimetric analysis (TGA) was virtually carried out both in air and N₂ atmosphere by the scraped powders of vapor-deposited CsSnBr₃ film with thickness of about 1 μm (Figure S3, in Supporting Information). The initial decomposing temperature of CsSnBr₃ is as high as 405 °C

probably due to partial release of bromine, proving its extremely high thermal stability, which is most available for optoelectronic devices.

To demonstrate the potential for applications in planar structure electrically driven lasers, the ASE measurements on these CsSnX₃ films were carried out by exciting at 400 nm with a frequency-doubled Ti:sapphire femtosecond laser delivering 150 fs pulses at a 1 kHz repetition rate. Through a pinhole filter and a positive lens, the laser beam formed a 2.5 mm diameter spot, and was irradiated obliquely onto the surface of the samples. As shown in **Figure 3a**, face emission spectra were collected directly into the Fiber Optic Spectrometer. The PMMA films were spin-coated as an encapsulation layer to protect these CsSnX₃ film from degradation in ambient environment (see Experimental Section). All the pumping processes were carried out under ambient conditions at room temperature.

As shown in Figure 3b, the surface topography of CsSnBr_{0.5}I_{2.5} film is evaluated by AFM showing very smooth surface with the RMS of surface roughness at ≈2.5 nm in the 5 × 5 μm² areas. The characteristics of full surface coverage on substrate without pinholes, small grain sizes, and extremely smooth surface topography for as-formed CsSnBr_{0.5}I_{2.5} film (Figure S4, in Supporting Information) will help reduce loss and improve gain. The measured output emission spectra, input-output intensity and the FWHM as a function of increasing pump energy are

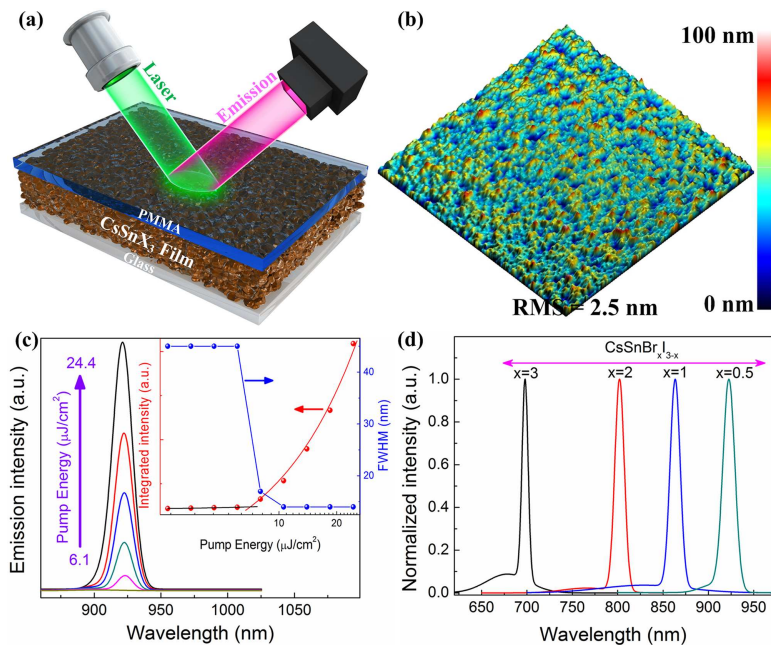


Figure 3. a) Schematic configuration of the sample and the face emission spectra collection. b) The 3D AFM image of the CsSnBr_{0.5}I_{2.5} film. c) Development of emission spectra for the CsSnBr_{0.5}I_{2.5} film with increasing pump energy. d) The normalized ASE spectra for CsSnBr_xI_{3-x} films fabricated by vapor deposition. The experiments were conducted with 400 nm pump pulses (150 fs, 1 kHz) under ambient conditions at room temperature.

shown in Figure 3c. At low pump energy, only a SE peak at 915 nm with the FWHM about 45 nm is observed. When the pump intensity exceeds the threshold, the spectral narrowing, that is, ASE, emerges at 923 nm while the FWHM dramatically decreased to about 14 nm at 10.6 $\mu\text{J cm}^{-2}$. The FWHM remains constant when the pump energy is further increased. Clearly, there is an obvious threshold at about $7 \pm 2 \mu\text{J cm}^{-2}$ in the input-output curve as shown in the inset of Figure 3c. The reason why ASE can be achieved in the CsSnBr_{0.5}I_{2.5} film is that the spontaneously emitted photons transmitted along gain media are amplified by stimulated emission. Owing to the stronger self-absorption, ASE does not occur at the SE peak wavelength 915 nm but 923 nm where the optical gain and absorption are balanced.

Finally, ASE from other CsSnX₃ gain media containing pure and mixed halides was also observed which proves the facile wavelength tunability through halide substitution. Figure 3d shows that the ASE peak could be tuned at room temperature from 697 to 923 nm by varying the bromide and iodide compositions to obtain CsSnBr₃, CsSnBr₂I, CsSnBrI₂, and CsSnBr_{0.5}I_{2.5} thin films. Their ASE thresholds were determined to be 25 ± 5 , 20 ± 4 , 14 ± 4 , and $7 \pm 2 \mu\text{J cm}^{-2}$, respectively by using a 400 nm pumping wavelength (150 fs, 1 kHz) (Figure S5, in Supporting Information). The ASE from the CsSnCl_xBr_{3-x} films have not been observed probably concerning with the high ASE threshold associated with the rough film morphology and high defect density, which lead to above the damage threshold (above the laser power range used). These CsSnX₃ films prepared by vapor deposition exhibit strong

optically and electrically pumped spontaneous emission, which are important characteristics for realizing electrically pumped lasers.

The optically pumped ASE threshold of gain media is usually used to estimate its minimum threshold current density of lasing under electrical pumping.^[33] As mentioned above, a lasing threshold as low as $7 \mu\text{J cm}^{-2}$ was obtained from optically pumped CsSnBr_{0.5}I_{2.5} film, corresponding to a photon density of about 10^{18} cm^{-3} . An equivalent density of excitons may be formed by an injection current density J_{th} , estimated using the equation: $J_{\text{th}} = qdn/\chi\tau$, where q is the electron charge, d is the recombination section of the active layer, n is the threshold photon density, τ is the radiative lifetime, and χ is the ratio of radiative singlet excitons to the total number of excitons formed by electrical injection. If the present PeLED architectures can be perfectly converted into an efficient, low capacitance LED that does not substantially increase the optical loss and maintains balanced charge carrier recombination under electrical pumping, the results here suggest that threshold current densities $J_{\text{th}} \approx 320 \text{ A cm}^{-2}$ may be within reach. Furthermore, by introducing an external optical cavity, the optically pumped lasing threshold of gain media can be drastically reduced, corresponds to a lower threshold current density easier to implement.

In previous reports, all the PeLEDs based on CsPbBr₃, MAPbBr₃, FAPbBr₃, or CsSnI₃ employed organic materials as holes transport layer (HTL), electrons transport layer (ETL) or holes blocking layer (HBL), which cannot withstand the large current density of lasing under electrical pumping.^[13,20] In order to try to meet the above required current density, all-inorganic architecture of PeLEDs should be established including perovskite, ETL and HTL. In this work, as shown in Figure 4a, the CsSnBr₃-based PeLEDs were fabricated with the structure of Glass/ITO/LiF (4 nm)/CsSnBr₃ (50 nm)/LiF (8 nm)/ZnS (30 nm)/Ag (100 nm), which has an effective area of about $3.4 \times 3.3 \text{ mm}^2$. Here, the ZnS layer was used as ETL as well as HBL due to the large barrier between the ionization potential level of CsSnBr₃ and the conductive band of ZnS, as shown in Figure 4b.^[19] The structure of “Insulator–Perovskite–Insulator” (IPI), namely “LiF/CsSnBr₃/LiF”, is employed, which has been described in details elsewhere in our publication.^[34] Under the applied voltage, holes and electrons will tunnel through LiF layers into CsSnBr₃ film respectively, recombine with each other radiatively, emitting light in all directions at last. Herein, all layers of the CsSnBr₃-based PeLEDs are inorganic materials, and thermally deposited on an indium-tin oxide (ITO)-coated patterned glass substrate in a vacuum chamber respectively. Typical electroluminescence (EL) and PL spectra are shown in Figure 4d. A strong red EL, centered at 672 nm and with a narrow full-width-at-half-maximum (FWHM) of $\approx 54 \text{ nm}$, could be measured, which is slightly red-shifted compared to the PL of the CsSnBr₃ film, centered at 670 nm and with a FWHM of about 56 nm. Therefore, it can be confirmed that the light emission of the PeLED originates from the CsSnBr₃ layer. The inset in

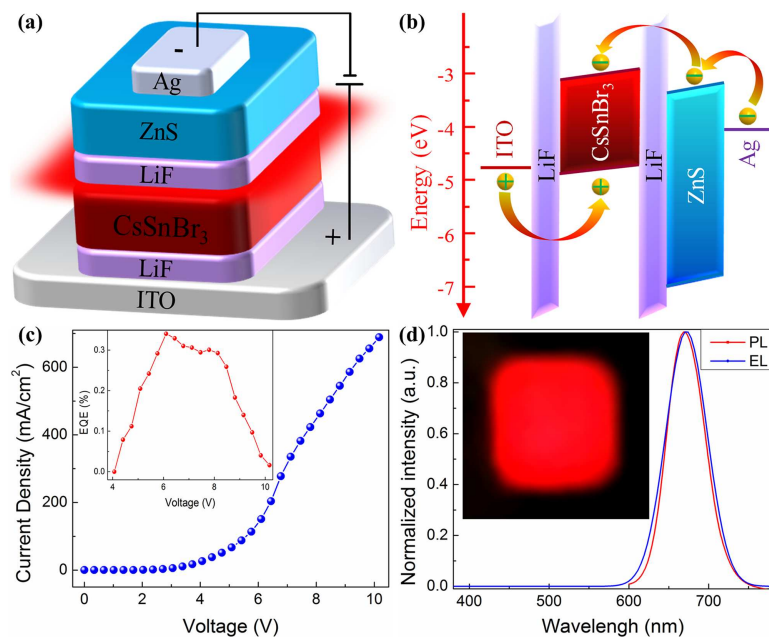


Figure 4. a) Device structure of the CsSnBr₃-based PeLED. b) Energy-level diagram of materials in the CsSnBr₃-based PeLED. c) The *J*-*V* characteristics and EQE performance for the CsSnBr₃-based PeLED. d) The normalized PL spectrum and normalized EL spectrum. The inset shows a representative photo of a functional CsSnBr₃-based PeLED.

Figure 4d shows a representative photo of a functional CsSnBr₃-based PeLED under 7 V of applied potential. The device emitted uniform red light throughout the whole active device area. Figure 4c presents the current density versus voltage (*J*-*V*) and EQE characteristics of the CsSnBr₃-based PeLED. As shown in Figure 4c, the typical *J*-*V* curve shows that the PeLED turns on under a low voltage bias value of about 4 V. After the device is turned on, the current density increases rapidly by orders of magnitude, accompanying with increased EQE and the peak EQE of ≈0.34% is obtained at about 6.1 V. In addition, the CsSnBr₃-based PeLED exhibited the highest luminance of about 172 cd m⁻² at 8.1 V and the maximum current efficiency (CE) of about 0.65 cd A⁻¹ at 6.1 V (Figure S6, in Supporting Information). In addition, the CsSnBr₃-based PeLED could continuously operate around 100 min under a constant applied voltage of about 6 V in a nitrogen-filled glove box (Figure S7, in Supporting Information). Considering the characteristics of small grain sizes and extremely smooth surface topography for the vapor deposited CsSnBr₃ layer, it will lead to smaller exciton diffusion length, helping reduce leakage current and improving current efficiency in PeLEDs.^[35] Here, the maximum current density values of the CsSnBr₃-based PeLED are not more than 1 A cm⁻² mainly due to the decomposition of the CsSnBr₃ layer caused by Joule heating effect.

To explore the maximum of current density passed through CsSnBr₃ film, the above PeLED with the small emission area of CsSnBr₃ is fabricated to avoid the heat accumulation and the consequent breakdown. In our experiment, the device was prepared with a very small effective area of about 0.1 × 0.1 mm², shown in Figure 5. This PeLED stays undestroyed even when the current density reaches as high as 915 A cm⁻² at about 28 V,

which shows the tolerance of CsSnBr₃ for high current density probably benefited from its high thermostability. Although the injected current density passed through PeLEDs reached the threshold current density estimated from ASE threshold of CsSnBr₃, the lasing actions of PeLEDs were still not observed. The EL intensity of PeLEDs with the small emission area increased rapidly with the increase of the applied voltage, and decreased dramatically when the voltage is over 9 V. The decrease of the EL intensity at high voltages probably derived from the electric field-induced exciton dissociation or the decomposition of the CsSnBr₃ layer possibly resulted from Joule heating effect or electric field-induced ionic migration. The EL spectra of this small area device at different voltages were directly collected by a fiber optic spectrometer as shown in the inset in Figure 5. As the device turned on at about 5 V, a typical EL spectrum centered at 672 nm with a FWHM of about 54 nm was obtained. Unfortunately, spectral narrowing effect did not occur until the device is breakdown. In order to estimate the EQE of the small area device, the EL and PL spectra of the CsSnBr₃ film were collected separately under the same measurement conditions. Assuming that the collection efficiency of the fiber optic system is equal and the absorption coefficient of the CsSnBr₃ film close to 100%, when PL and EL

intensity is adjusted to equal, the ratio of the EQE to PLQY can be estimated as: $\text{EQE}/\text{PLQY} = (q \times P_{400}) / (I \times h\nu)$, where *q* is the electron charge, *P*₄₀₀ is the pump power of the laser (400 nm), *I* is the current value, *hν* is the photon energy (here, *hν* = 3.1 eV).^[36] When the applied voltage is 5 V, the corresponding current in the device is about 3.8 mA and the corresponding *P*₄₀₀ about 175 μW, and then the calculated EQE is about 0.135%. When the applied voltage is 9 V (the corresponding current is about 19.3 mA and the corresponding *P*₄₀₀ about 425 μW), the calculated EQE reduces to about 0.064%.

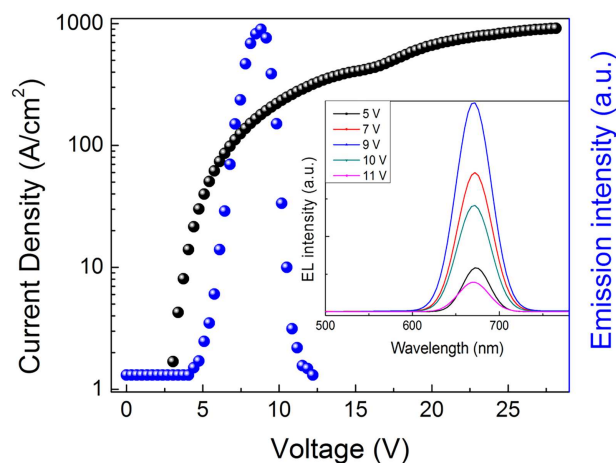


Figure 5. The *J*-*V* characteristics and the EL emission intensity for the device with a small effective area. The inset shows the EL spectra of the device with a small effective area at different voltages.

In fact, the estimated threshold current density for lasing of the CsSnBr₃-based PeLEDs is the lowest limit owing to the ignorance of additional losses in the device, such as the loss derived from metal contact, carrier injection and non-radiative recombination. For example, the loss from metal contact in PeLEDs comes from the absorption of metallic cathode by which the light is reflected, and the metallic film also leads to the PL quenching of the emission centers in the scope of several nanometers. The imbalance of injected holes and electrons leads to leakage current, which results in the lower current efficiency of devices, and the dissociation of excitons under applied voltages are sure to seriously reduce the PL and ASE intensity of perovskite film.^[4] Our previous work also demonstrated the quenching of ASE intensity for the MAPbI₃ film under high external electric field.^[37] Subject to these additional losses, it is understandable for the failure of electrically pumped lasing in PeLEDs in our experiment, although the minimum current density required for lasing behaviors has been reached. Like cases of organic light-emitting diodes and the lasing from the organic gain media, many efforts could be done to reduce or avoid these additional losses, such as pulsed electrical pumping of very small structures, optimized optical structure design to reduce the negative effects caused by contacts, even exploiting light-emitting transistors to avoid metal contact.^[38–40] Only through the delicate design for the architecture of PeLEDs, the additional losses in devices could be greatly reduced, even avoided, and then the current density required for lasing of perovskite films could be achieved, and finally the electrically pumped LDs based on the perovskite materials could be expected. How to avoid these additional losses in devices will be investigated in future, which is beyond the scope of this work. In this article, we demonstrate that both high current endurance of all-inorganic hetero-structured PeLEDs and the lower ASE threshold of smooth CsSnX₃ films with high quality promise the feasibility of electrically pumped LDs based on CsSnX₃ films. The tolerance of CsSnBr₃ for high current density primarily derived from the high thermostability and high carrier mobility characteristics. It provides a bright prospect for realizing electrically pumped lasers if the obstacle of non-radiative quenching at high carrier densities such as field-induced exciton dissociation and auger recombination can be cleared.

In conclusion, all vapor-deposited Sn-based perovskites have been used to fabricate PeLEDs and showed ASE behaviors. All-inorganic hetero-structured PeLED based on CsSnBr₃ is demonstrated by all vacuum vapor-deposition, which exhibited a maximum EQE of $\approx 0.34\%$, and could sustain high current density up to 915 A cm^{-2} with the small emission zone as 0.01 mm^2 . By vapor deposition, extremely smooth, uniform and full coverage CsSnX₃ films with small grain size of about 60 nm were achieved, which show the low threshold ($\approx 7 \mu\text{J cm}^{-2}$) ASE and tunable lasing emissions in broader wavelengths (697–923 nm) through different halogen substitutions. These CsSnX₃ perovskites with high optical gain, carrier mobility and current density carrying capability characteristics exhibit great potential for demonstrating electrically pumped lasers.

Experimental Section

Perovskite Film Fabrication: To prepare the samples, the pre-cleaved glass substrates or indium-tin oxide (ITO)-coated patterned glass substrates were cleaned with deionized water and organic solvents, and then exposed to a UV-ozone ambient for 5 min. For the preparation of the CsSnX₃ films, taking CsSnBr₃ film for example, the desired thicknesses of SnBr₂ (50 nm) and CsBr (45 nm) with about equally stoichiometric ratio were sequentially deposited in a vacuum chamber at a rate of about $0.4\text{--}0.5 \text{ \AA s}^{-1}$ under a pressure $1 \times 10^{-3} \text{ Pa}$. After deposition, the substrates were transferred into a nitrogen-filled glove box and then annealed at 100°C for 60 min to form the perovskite layer. For the preparation of the all-inorganic CsSnBr₃-based PeLEDs with the structure of Glass/ITO/LiF (4 nm)/CsSnBr₃ (50 nm)/LiF (8 nm)/ZnS (30 nm)/Ag (100 nm), all layers were sequentially deposited in a vacuum chamber at a rate of about 0.5 \AA s^{-1} under a pressure of $1 \times 10^{-3} \text{ Pa}$. For measuring the ASE of these CsSnX₃ films, polymethylmethacrylate (PMMA) dissolved in the chlorobenzene solution (20 mg mL^{-1}) were spin-coated at 1000 rpm for 30 s onto the substrates and then annealed at 100°C for 10 min to complete device preparation. The PMMA films were spin-coated as an encapsulation layer to protect the CsSnX₃ films from degradation in ambient conditions. The other CsSnX₃ perovskite films containing pure and mixed halides were prepared with the desired thicknesses of SnX₂ and CsX of about equally stoichiometric ratio.

Device Characterization: Film thickness of the samples was measured by ellipsometry (SE MF-1000, Korea). The surface of the CsSnX₃ films was investigated by scanning electron microscopy (SEM, Quanta 250, FEI). Surface topography of the CsSnX₃ films was measured by an atomic force microscope (AFM, NT-MDT, Russia). The crystalline structure of the CsSnX₃ films on glass substrate was determined by X-ray diffraction (XRD, D/MAX-2400, Rigaku, Japan). The absorption and PL spectra were obtained by a UV-vis spectrophotometer (HITACHI U-3010, Japan) and a fluorescence spectrometer (Fluoromax-4 spectrofluorometer), respectively. The PLQE of the CsSnX₃ films was measured using an integrating sphere. The CsSnBr₃ powder peeled off from the substrate, were analyzed by thermogravimetric analysis (TGA) with Mettler TGA Instrument using a $10^\circ\text{C min}^{-1}$ ramp up to 800°C both in air and N₂ atmosphere with a steady flow rate of 10 mL min^{-1} . The femtosecond pulses were delivered from the frequency doubled output of a Ti:sapphire femtosecond laser. Face emission spectra were collected by a fiber-optic spectrometer (Ocean Optics Spectra Suite, USB2000). The characteristics of the all-inorganic CsSnBr₃-based PeLEDs were measured using a computer-controlled source meter (Keithley 2602) and a calibrated silicon photodiode. The EL spectra of the large area device were measured by a PR650 spectrometer and the EL spectra for the small area device were directly collected by a fiber optic spectrometer (Ocean Optics Spectra Suite, USB2000). All measurements were carried out under ambient conditions at room temperature.

Supporting Information

Supporting Information is available from the Wiley Online Library or from the author.

Acknowledgements

This work was financially supported by National Natural Science Foundation of China (Grant No. 11574248), International Cooperation by Shaanxi (Grant No. 2015KW-008), China Postdoctoral Science Foundation (Grant No. 2016M590947), the Fundamental Research Funds for the Central Universities (Grant No. xjj2016031), the National Natural Science Foundation of China (Grant No. 61505161), the Natural Science Basic Research Plan of Shaanxi Province (Grant No. 2017JM6064), and the Scientific Research Plan Projects of Shaanxi Education Department (Grant No. 17JK0700). The SEM and TEM work was done at International Center for Dielectric Research (ICDR), Xi'an Jiaotong University, Xi'an, China.

Conflict of Interest

The authors declare no conflict of interest.

Keywords

amplified spontaneous emission, electrically pumped lasers, lead-free cesium tin halide perovskite, perovskite light-emitting diodes, vapor deposition

Received: February 27, 2018

Revised: March 7, 2018

Published online:

- [1] F. Grosshans, G. Van Assche, J. Wenger, R. Brouri, N. J. Cerf, P. Grangier, *Nature* **2003**, 421, 238.
- [2] M. T. Hill, M. Marell, E. S. P. Leong, B. Smalbrugge, Y. C. Zhu, M. H. Sun, P. J. van Veldhoven, E. J. Geluk, F. Karouta, Y. S. Oei, R. Notzel, C. Z. Ning, M. K. Smit, *Opt. Express* **2009**, 17, 11107.
- [3] V. G. Kozlov, V. Bulovic, P. E. Burrows, S. R. Forrest, *Nature* **1997**, 389, 362.
- [4] I. D. W. Samuel, G. A. Turnbull, *Chem. Rev.* **2007**, 107, 1272.
- [5] S. Chenais, S. Forget, *Polym. Int.* **2012**, 61, 390.
- [6] C. F. Klingshirn, *Semiconductor Optics*, Springer-Verlag, Berlin, Heidelberg, New York **2007**.
- [7] E. Kannekoy-Asibu, Jr., *Principles of Laser Materials Processing*, Wiley, Hoboken, NJ, USA **2009**.
- [8] N. Tessler, D. J. Pinner, V. Cleave, D. S. Thomas, G. Yahioglu, P. Le Barny, R. H. Friend, *Appl. Phys. Lett.* **1999**, 74, 2764.
- [9] A. Kojima, K. Teshima, Y. Shirai, T. Miyasaka, *J. Am. Chem. Soc.* **2009**, 131, 6050.
- [10] M. Liu, M. B. Johnston, H. J. Snaith, *Nature* **2013**, 501, 395.
- [11] H. S. Jung, N. G. Park, *Small* **2015**, 11, 10.
- [12] W. S. Yang, J. H. Noh, N. J. Jeon, Y. C. Kim, S. Ryu, J. Seo, S. I. Seok, *Science* **2015**, 348, 1234.
- [13] S. A. Veldhuis, P. P. Boix, N. Yantara, M. Li, T. C. Sum, N. Mathews, S. G. Mhaisalkar, *Adv. Mater.* **2016**, 28, 6804.
- [14] B. R. Sutherland, E. H. Sargent, *Nat. Photonics* **2016**, 10, 295.
- [15] F. Deschler, M. Price, S. Pathak, L. E. Klüntberg, D. D. Jarausch, R. Higler, S. Hüttner, T. Leijtens, S. D. Stranks, H. J. Snaith, M. Atature, R. T. Phillips, R. H. Friend, *J. Phys. Chem. Lett.* **2014**, 5, 1421.
- [16] NREL, **2016**, <https://www.nrel.gov/pv/assets/images/efficiency-chart.png>
- [17] N. N. Wang, L. Cheng, R. Ge, S. T. Zhang, Y. F. Miao, W. Zou, C. Yi, Y. Sun, Y. Cao, R. Yang, Y. Q. Wei, Q. Guo, Y. Ke, M. T. Yu, Y. Z. Jin, Y. Liu, Q. Q. Ding, D. W. Di, L. Yang, G. C. Xing, H. Tian, C. H. Jin, F. Gao, R. H. Friend, J. P. Wang, W. Huang, *Nat. Photonics* **2016**, 10, 699.
- [18] N. K. Noel, S. D. Stranks, A. Abate, C. Wehrenfennig, S. Guarnera, A. A. Haghghirad, A. Sadhanala, G. E. Eperon, S. K. Pathak, M. B. Johnston, A. Petrozza, L. M. Herz, H. J. Snaith, *Energy Environ. Sci.* **2014**, 7, 3061.
- [19] D. Moghe, L. Wang, C. J. Traverse, A. Redoute, M. Sponseller, P. R. Brown, V. Bulović, R. R. Lunt, *Nano Energy* **2016**, 28, 469.
- [20] W. W. L. Hong, Y. C. Huang, C. Y. Chang, Z. C. Zhang, H. R. Tsai, N. Y. Chang, Y. C. Chao, *Adv. Mater.* **2016**, 28, 8029.
- [21] G. Xing, M. H. Kumar, W. K. Chong, X. Liu, Y. Cai, H. Ding, M. Asta, M. Grätzel, S. Mhaisalkar, N. Mathews, T. C. Sum, *Adv. Mater.* **2016**, 28, 8191.
- [22] F. Wang, J. Ma, F. Xie, L. Li, J. Chen, J. Fan, N. Zhao, *Adv. Funct. Mater.* **2016**, 26, 3417.
- [23] C. C. Stoumpos, C. D. Malliakas, M. G. Kanatzidis, *Inorg. Chem.* **2013**, 52, 9019.
- [24] Z. Xiao, Y. Zhou, H. Hosono, T. Kamiya, *Phys. Chem. Chem. Phys.* **2015**, 17, 18900.
- [25] X. Qiu, B. Cao, S. Yuan, X. Chen, Z. Qiu, Y. Jiang, Q. Ye, H. Wang, H. Zeng, J. Liu, M. G. Kanatzidis, *Sol. Energy Mater. Sol. Cells* **2017**, 159, 227.
- [26] W. Li, J. Li, J. Li, J. Fan, Y. Mai, L. Wang, *J. Mater. Chem. A* **2016**, 4, 17104.
- [27] K. P. Marshall, M. Walker, R. I. Walton, R. A. Hatton, *Nat. Energy* **2016**, 1, 16178.
- [28] I. Chung, B. Lee, J. Q. He, R. P. H. Chang, M. G. Kanatzidis, *Nature* **2012**, 485, 486.
- [29] C. Bi, Y. Shao, Y. Yuan, Z. Xiao, C. Wang, Y. Gao, J. Huang, *J. Mater. Chem. A* **2014**, 2, 18508.
- [30] T. C. Jellicoe, J. M. Richter, H. F. Glass, M. Tabachnyk, R. Brady, S. E. Dutton, A. Rao, R. H. Friend, D. Credgington, N. C. Greenham, M. L. Bohm, *J. Am. Chem. Soc.* **2016**, 138, 2941.
- [31] K. Shum, Z. Chen, J. Qureshi, C. Yu, J. J. Wang, W. Pfenninger, N. Vockic, J. Midgley, J. T. Kenney, *Appl. Phys. Lett.* **2010**, 96, 221903.
- [32] N. K. Noel, A. Abate, S. D. Stranks, E. S. Parrott, V. M. Burlakov, A. Goriely, H. J. Snaith, *ACS Nano* **2014**, 8, 9815.
- [33] S. Colella, M. Mazzeo, A. Rizzo, G. Gigli, A. Listorti, *J. Phys. Chem. Lett.* **2016**, 7, 4322.
- [34] Y. Shi, W. Wu, H. Dong, G. Li, K. Xi, G. Divitini, C. Ran, F. Yuan, M. Zhang, B. Jiao, X. Hou, Z. Wu, *Adv. Mater.* **2018**, <https://doi.org/10.1002/adma.201800251>.
- [35] H. C. Cho, S. H. Jeong, M. H. Park, Y. H. Kim, C. Wolf, C. L. Lee, J. H. Heo, A. Sadhanala, N. Myoung, S. Yoo, S. H. Im, R. H. Friend, T. W. Lee, *Science* **2015**, 350, 1222.
- [36] X. Hu, H. Zhou, Z. Jiang, X. Wang, S. Yuan, J. Lan, Y. Fu, X. Zhang, W. Zheng, X. Wang, X. Zhu, L. Liao, G. Xu, S. Jin, A. Pan, *ACS Nano* **2017**, 11, 9869.
- [37] F. Yuan, Z. Wu, H. Dong, B. Xia, J. Xi, S. Ning, L. Ma, X. Hou, *Appl. Phys. Lett.* **2015**, 107, 261106.
- [38] H. Yamamoto, H. Kasajima, W. Yokoyama, H. Sasabe, C. Adachi, *Appl. Phys. Lett.* **2005**, 86, 3.
- [39] M. Reufer, S. Riechel, J. M. Lupton, J. Feldmann, U. Lemmer, D. Schneider, T. Benstem, T. Dobbertin, W. Kowalsky, A. Gombert, K. Forberich, V. Wittwer, U. Scherf, *Appl. Phys. Lett.* **2004**, 84, 3262.
- [40] T. Oyamada, H. Sasabe, C. Adachi, S. Okuyama, N. Shimoyi, K. Matsushige, *Appl. Phys. Lett.* **2005**, 86, 3.